


Electron-lattice coupling effects in nonadiabatic polarization switching of charge-order-induced ferroelectrics

Yubo Qi  and Karin M. Rabe*Department of Physics & Astronomy, Rutgers University, Piscataway, New Jersey 08854, USA* (Received 22 June 2021; revised 20 July 2022; accepted 22 August 2022; published 19 September 2022)

We carry out first-principles density-functional-theory calculations to investigate the possibility of nonadiabatic switching (purely electronic hopping without structural change) in charge-order-induced ferroelectrics. In charge-order-induced ferroelectrics, polarization switching can in principle occur through nonadiabatic interionic electron hopping with an ultrafast speed. However, lattice relaxation for a specific charge-ordering state can “lock” that state in, making nonadiabatic switching to a different charge-ordering variant energetically prohibitive; whether nonadiabatic switching on electronic time scales can occur thus depends on the strength of lattice-electron coupling. In this work, we propose a simple model predicting the possibility of nonadiabatic switching based on structural analysis. Specifically, we point out that electric field driven nonadiabatic electron hopping is possible in charge-order-induced ferroelectrics whose primary coupling mode is off-centering displacement, rather than polyhedral breathing. We carry out calculations and analysis on three different prototype charge-ordering materials, including the (theoretically designed) $(\text{SrVO}_3)_1(\text{LaVO}_3)_1$ superlattice, LuFe_2O_4 , and Fe_3O_4 . All the results support our theory and are also in accord with experimental observations. These results show the critical role of electron-lattice coupling in nonadiabatic polarization switching in charge-order-induced ferroelectrics, providing guidance for the design and discovery of “electronic ferroelectrics” with ultrafast polarization switching on electronic rather than lattice time scales.

DOI: [10.1103/PhysRevB.106.125131](https://doi.org/10.1103/PhysRevB.106.125131)

I. INTRODUCTION

In strongly correlated materials, the charges in transition metal ions can disproportionate and form an ordered arrangement. This charge ordering (CO) breaks symmetries of the crystal and may induce ferroelectricity [1–4]; this behavior has been experimentally observed in Fe_3O_4 [5,6]. The search for additional CO-induced ferroelectric materials has attracted lively interest. Proposed systems include $\text{Pr}_x\text{Ca}_{1-x}\text{MnO}_3$ [2,7–14], rare-earth nickelates (RNiO_3) [15,16], rare-earth manganites RMn_2O_5 [17–24], and several superlattice structures [25–27].

In CO-induced ferroelectrics, polarization switching can in principle occur through nonadiabatic interionic electron hopping alone, without structural change. CO-induced ferroelectrics are thus natural candidates for electronic ferroelectrics, which have recently attracted considerable interest for ultrafast switching applications since switching of the electronic state can occur on time scales much shorter than the lattice-driven switching in conventional ferroelectrics [5,28,29]. However, coupling of the CO to the lattice will in general lead to structural relaxation that “locks in” a particular CO state, making nonadiabatic switching to a different CO variant energetically prohibitive.

The coupling between the CO state and the lattice gives rise to two adiabatic potential energy surfaces as shown in Fig. 1(a). In close analogy to the Franck-Condon process, a given CO state with full structural relaxation will be lower in energy than the oppositely polarized state obtained by

electric-field-driven purely electronic hopping (this excited electronic state is referred to here as the “electronically” oppositely polarized CO state). This energy difference ΔE is directly related to the strength of the CO-lattice coupling. Under an electric field, the relevant thermodynamic quantity is the electric enthalpy $\Delta H = V E_{el} \Delta P$, where V is the volume and ΔP is the difference between the polarization of the two CO states. As shown in Fig. 1(b), applying a positive electric field E_{el} reduces the electric enthalpy of the up-polarized CO state relative to the down-polarized CO state.

To induce nonadiabatic switching to the oppositely polarized charge-ordering variant, the electric field has to be larger than $\Delta E / \Delta PV$ [Fig. 1(c)]. If ΔE is too large, nonadiabatic switching will require an unreasonably large (above the breakdown field) electric field. Therefore, the strength of the CO-lattice coupling, which determines ΔE , plays a crucial role in determining the possibility of nonadiabatic purely electronic switching.

Here, we propose a simple structural analysis model to predict the possibility of ultrafast nonadiabatic switching. Specifically, we identify two main types of relevant lattice modes, polyhedral breathing (PB) and off-centering displacement (OD), for which the strength of coupling to CO is expected to be quite different. Typically, the PB mode couples to the CO state strongly, thus prohibiting nonadiabatic switching. On the other hand, in the CO materials in which OD is the primary lattice mode coupled to the CO state, ΔE is typically much smaller, opening the possibility of nonadiabatic switching. In this work, we select the $(\text{SrVO}_3)_1(\text{LaVO}_3)_1$

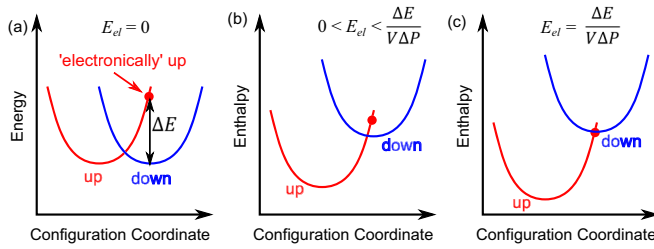


FIG. 1. (a) Schematic plot showing the adiabatic potential surfaces for the up-polarized and down-polarized states and the energy difference between the optimized down-polarized state and the excited “electronically” up-polarized state with no change in atomic positions. (b) and (c) Changes of the electric enthalpy profiles under increasing electric field.

superlattice as an illustrative example, due to its simple structure, for explaining different types of lattice modes and the CO-lattice coupling strength. Next, we apply our model to predict the nonadiabatic switchabilities of prototype CO materials, including the $(\text{SrVO}_3)_1(\text{LaVO}_3)_1$ superlattice, LuFe_2O_4 [30–36], and Fe_3O_4 [5,6,37,38], by performing structural analysis and confirming the results by first-principles calculations. All of the results and predictions based on our model are in accord with experimental observations. The model also provides insights into a long-standing puzzle: why ultrafast switching, or even normal lattice-based switching, has not been observed in some prototype charge-ordering materials, such as LuFe_2O_4 . This work aims to deepen our understanding of nonadiabatic polarization switching in CO-induced ferroelectrics and provides valuable guidance for designing and realizing electronic ferroelectricity with polarization switching on electronic time scales.

II. LATTICE MODE ANALYSIS

First, we introduce the two lattice modes—the PB mode and the OD mode—that couple most strongly to the CO states. Since the radius of the low-valence cation is larger than that of the high-valence cation, we expect a polyhedral breathing (magnitude denoted by Q_{PB}) lattice distortion, with expansions of the coordination polyhedra surrounding the low-valence cations and contractions of the coordination polyhedra surrounding the high-valence cations. Such an ionic-size-induced polyhedral breathing mode is characteristic of CO materials and has been widely discussed [16,39–41]. Off centering displacement (magnitude denoted by Q_{OD}) is the other lattice distortion that is expected to couple to the ionic size difference in charge ordering, with the smaller cation showing a greater tendency to displace. We note that the octahedral rotation distortions, which are ubiquitous in perovskite oxides, do not couple strongly to the ionic size difference. This was established in Ref. [25], and the octahedral rotation distortions are not discussed further in the present work.

Of the two modes (PB and OD) most strongly coupled to the CO states, the PB mode is expected to have a substantially stronger coupling than the OD mode. For relaxation with a PB mode, most or all of the transition metal-anion bonds can achieve their preferred length, maximizing the energy gain.

On the other hand, for relaxation with an OD mode, displacement of the cation cannot place it a preferred distance from all the surrounding anions, resulting in a much smaller net energy gain. In the following part, we present first-principles results [see Supplemental Material (SM) Sec. I for computational details [42]] on the $(\text{SrVO}_3)_1(\text{LaVO}_3)_1$ superlattice to provide an intuitive illustration of different coupling strengths of the PB and OD modes.

In previous theoretical work, it was shown that at low temperatures, the $(\text{SrVO}_3)_1(\text{LaVO}_3)_1$ superlattice is a Mott insulator with vanadium ions disproportionating into V^{3+} and V^{4+} [25]. This superlattice can adopt three different CO patterns which have quite similar energies when the structure is fully relaxed [25]. Specifically, there is a layered charge-ordering (LCO) pattern (see SM Sec. II for the structure) that can be stabilized over the other two competing patterns by strain or an applied electric field (see SM Sec. III for more discussion); this pattern, combining with the symmetry breaking by the cation order in the superlattice, breaks symmetry to a polar state.

Since the superlattice stacking constrains the in-plane lattice parameter to be equal in the V^{3+} and V^{4+} layers, the oxygen octahedron surrounding a V^{3+} ion elongates in the direction perpendicular to the layers and the one surrounding a V^{4+} ion shortens [Fig. S1(a)]. The PB amplitude can be measured by the ratio of the heights of the two octahedra as

$$R = \frac{L_1}{L_2}. \quad (1)$$

Conversely, if we fix the value of R , the V^{4+} ion will tend to favor the site with the smaller value of L . The OD mode also contributes to the structural relaxation of the LCO $(\text{SrVO}_3)_1(\text{LaVO}_3)_1$ superlattice [Fig. S1(b)], with displacements of V_1 and V_2 in opposite directions, in each case from the SrO layer to the LaO layer (see SM Sec. IV for more discussion).

Our density-functional-theory (DFT) calculations show that the mode magnitudes of the optimized down-polarized $(\text{SrVO}_3)_1(\text{LaVO}_3)_1$ superlattice structure are $R_0 = 0.91$, $Q_{OD}(\text{V}^{3+}) = 0.04 \text{ \AA}$ and $Q_{OD}(\text{V}^{4+}) = 0.09 \text{ \AA}$, consistent with the larger size of V^{3+} as discussed above. To investigate the coupling of different lattice modes to the CO states, we generate energy landscapes as described in SM Sec. I for various R values in the plane of $Q_{OD}(\text{V}_1)$ and $Q_{OD}(\text{V}_2)$ [43–45]. We use occupation matrix control to generate starting electronic states with $\text{V}_1, \text{V}_2 = \text{V}^{3+}, \text{V}^{4+}$ and $\text{V}_1, \text{V}_2 = \text{V}^{4+}, \text{V}^{3+}$, respectively, relax the structures with fixed PB and OD modes, and identify the lower-energy CO state for each structure.

We begin with the energy landscape for $R = 1$. Electronic correlation promotes localization of the electron into a single ionic orbital (see SM Sec. V for the occupation matrices). Even with polyhedral breathing completely suppressed and $Q_{OD}(\text{V}_1) = Q_{OD}(\text{V}_2)$, we find that charge disproportionation is still energetically favorable. With $Q_{OD}(\text{V}_1) \neq Q_{OD}(\text{V}_2)$, the preferred arrangement of the V^{3+} and V^{4+} will be determined by the OD modes. The resulting energy landscape is shown in Fig. 2(a). In the upper part, we have

$$Q_{OD}(\text{V}_1) < Q_{OD}(\text{V}_2) \Rightarrow \text{V}_1 = \text{V}^{3+} \text{ and } \text{V}_2 = \text{V}^{4+}, \quad (2)$$

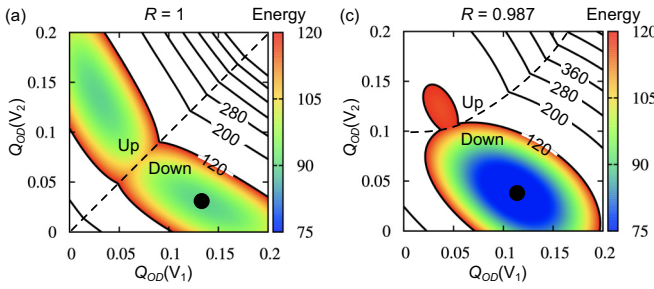


FIG. 2. Energy landscapes as functions of $Q_{OD}(V_1)$ and $Q_{OD}(V_2)$, with (a) $R = 1$ and (b) $R = 0.987$.

which corresponds to an up-polarized CO state. Similarly, the lower part corresponds to a down-polarized CO state. As R decreases to 0.987 [Fig. 2(b)], the oxygen octahedron associated with V_1 compresses, favoring V^{4+} . The effect on the energy landscape is that the dashed line, which represents the boundary of the up- and down-polarized regions, moves toward the left corner, indicating that $Q_{OD}(V_2)$ needs to exceed $Q_{OD}(V_1)$ by a critical amount to stabilize the up-polarized state. Also, the local minimum corresponding to the up-polarized CO state becomes quite shallow. If R decreases further to 0.981 (not shown in Fig. 2), the up-polarized CO state completely loses its stability; that is, no matter how much bigger $Q_{OD}(V_2)$ is than $Q_{OD}(V_1)$, V^{3+} will favor the V_2 site. This is consistent with our expectation that a given CO state is stabilized by lattice distortion, with PB modes being the most strongly coupled and leading to the greatest energy gains relative to other distortions such as OD.

III. RESULTS AND DISCUSSION

As discussed in the introduction, the strength of the coupling between the CO state and the lattice determines ΔE , the energy difference between a CO state with full structural relaxation and the oppositely electronically polarized CO state, and the value of ΔE determines whether nonadiabatic switching is possible. In the $(\text{SrVO}_3)_1(\text{LaVO}_3)_1$ superlattice, we showed above that as R gets far away from 1, the energetically unfavorable CO state (up-polarized CO state for $R < 1$) is not even locally stable and we cannot calculate ΔE directly. Here, we estimate ΔE based on the extrapolation of available data. We generate intermediate structures with a linear interpolation between the fully optimized up-polarized structure ($\lambda = 0$, $R = 1.095$) and fully optimized down-polarized structure ($\lambda = 1$, $R = 0.913$). For the structures with $\lambda < 0.6$, we calculate their energies with the up-polarized CO state (this is done by manipulating the occupation matrices) shown as red circles in Fig. 3(a). For the structures with $\lambda > 0.6$, we calculate their energies with the down-polarized CO state shown as blue circles in Fig. 3(a). We find that for each CO state, the energy has an almost perfect quadratic relationship with λ (the correlation coefficient is 0.999679), which we use to extrapolate the energy profile for up-polarized CO state (red curve) to $\lambda = 1$ and the energy profile for down-polarized CO state (blue curve) to $\lambda = 0$. As shown in Fig. 3(a), the energy difference between the fully optimized down-polarized state and its corresponding “electronically up-polarized” state

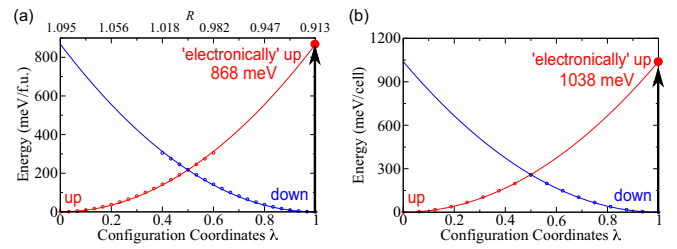


FIG. 3. Energies of the up-polarized (red) and down-polarized (blue) CO states of the structures interpolated between the fully optimized up-polarized structure ($\lambda = 0$) and fully optimized down-polarized structure ($\lambda = 1$).

is $\Delta E = 868$ meV/f.u.. Compensating such a large energy difference requires

$$E_{el} = \frac{\Delta E}{V \Delta P} = 22.7 \text{ MV/cm}, \quad (3)$$

which is much larger than the breakdown field of almost all ferroelectrics [46,47].

To investigate the influence of the OD mode on the stability of a CO state, we consider the $(\text{SrVO}_3)_1(\text{LaVO}_3)_1$ superlattice with R artificially fixed to 1. The PB character is thus completely eliminated, and in zero applied field, the CO state, and thus the polarization, couples to the OD modes only. We begin with a down-polarized structure, in which the 4+ valence state is on the V_1 site, and then fully relax the structure. The lattice symmetry of the optimized down-polarized structure is broken by the off-centering displacements with $Q_{OD}(V_1) \neq Q_{OD}(V_2)$. We also calculate the energy of its corresponding “electronically up-polarized” CO state and find that $\Delta E = 109$ meV/f.u.. This can be balanced by an electric field above 1.92 MV/cm, a value readily accessible in a laboratory. This threshold electric field is much reduced compared with that in a PB-type CO material, consistent with weaker coupling of the OD displacement to the CO state.

The results based on the $(\text{SrVO}_3)_1(\text{LaVO}_3)_1$ superlattice structure suggest more generally that PB- and OD-type CO materials have different nonadiabatic switchabilities under an applied electric field. The primary lattice mode coupling to the CO state can be identified by analysis of the relaxed structure for a given CO state. In the following, we extend our predictions based on this structural analysis, with supporting first-principles calculations, to other prototype CO materials, such as LuFe_2O_4 and Fe_3O_4 , and discuss the implications of our theory to their different experimentally observed polarization switchabilities.

First, we discuss polarization switchability in LuFe_2O_4 . In 2005, Ikeda *et al.* demonstrated that LuFe_2O_4 has two oppositely polarized states, which can be obtained by cooling from a high-temperature centrosymmetric structure under oppositely directed electric fields [30,31,48]. The emergence of polarization was attributed to the disproportionation and ordered arrangement of Fe atoms [30–33]. These results made LuFe_2O_4 a promising candidate for CO-induced ferroelectricity. However, electric-field-induced polarization switching in LuFe_2O_4 has not been experimentally demonstrated, leading to a long-running debate about whether LuFe_2O_4 is indeed ferroelectric [34–36].

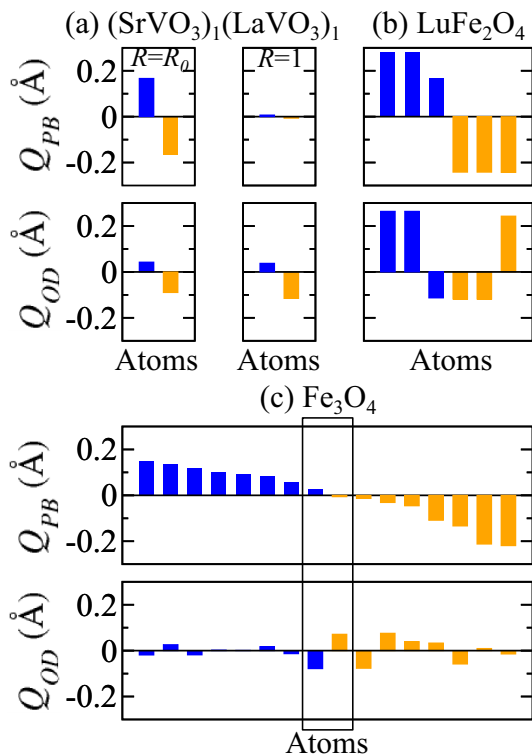


FIG. 4. Q_{PB} and Q_{OD} of the ions in (a) unconstrained ($R = R_0$) and constrained ($R = 1$) $(\text{SrVO}_3)_1(\text{LaVO}_3)_1$ superlattice, (b) LuFe_2O_4 , and (c) Fe_3O_4 . Each bar represents a transition metal ion in the primitive cell. The primitive cells of the $(\text{SrVO}_3)_1(\text{LaVO}_3)_1$ superlattice, LuFe_2O_4 , and Fe_3O_4 have 2, 6, and 16 nonequivalent transition metal ions, respectively. The blue and orange bars correspond to the lower valence (V^{3+} or Fe^{2+}) and higher valence states (V^{4+} or Fe^{3+}), respectively. The ions are ordered according to their values of Q_{PB} . The box in (c) shows a pair of Fe sites whose valence states can switch.

In the following, we perform an analysis of the previously reported structure [33] that demonstrates that LuFe_2O_4 is a PB-type CO material (see SM Sec. VI). To quantify the polyhedral breathing distortion, for each transition-metal-centered polyhedra, we define Q_{PB} as

$$Q_{PB}(i) = \sum_j (r_{ij} - \bar{r}), \quad (4)$$

where j runs over all the oxygen atoms bonded to the Fe ion i , r_{ij} is the distance from the center of the polyhedron containing the Fe ion i to the oxygen atom j , and \bar{r} is the average of all the r_{ij} in the entire unit cell. A negative Q_{PB} corresponds to a smaller polyhedron, and a positive Q_{PB} corresponds to a larger polyhedron. $R < 1$ for the $(\text{SrVO}_3)_1(\text{LaVO}_3)_1$ superlattice corresponds to $Q_{PB}(\text{V}_1) < 0$ and $Q_{PB}(\text{V}_2) > 0$, as shown in Fig. 4(a). In Fig. 4(b), we plot Q_{PB} and Q_{OD} for the six Fe ions in a LuFe_2O_4 primitive cell [33]. We can see that in LuFe_2O_4 , Q_{PB} for Fe^{2+} is noticeably larger than Q_{PB} for Fe^{3+} , with a difference even larger than that of the fully relaxed $(\text{SrVO}_3)_1(\text{LaVO}_3)_1$ superlattice [Fig. 4(a) $R = R_0$]. From this we conclude that the CO states in LuFe_2O_4 are strongly coupled to the PB mode.

The strong coupling of the PB mode to the CO states determined from the structural analysis indicates a large ΔE . We confirm this with first-principles calculations [analogous to the $(\text{SrVO}_3)_1(\text{LaVO}_3)_1$ superlattice case] in LuFe_2O_4 , as shown in Fig. 3(b). As expected, we find that ΔE for the nonadiabatic switching is large (1038 meV/cell), which corresponds to a 7.5 MV/cm electric field. This electric field is beyond the breakdown fields of most solid-state materials [46,47]. We confirm that the PB mode is responsible for the large ΔE by constraining the two polyhedra associated with the two Fe ions participating in the charge transfer to have the same volume (see SM Sec. VI for more details), and find that ΔE is reduced to 177 meV/cell, which corresponds to a much lower electric field of 1.3 MV/cm.

These results indicate that electric-field-induced nonadiabatic switching cannot occur in LuFe_2O_4 . Though we have not studied adiabatic switching or the possible effects of thermal vibrations, which in principle could assist switching, our results are consistent with and partially explain the fact that the $P - E$ loop has not been experimentally observed.

Next, we consider magnetite (Fe_3O_4), which is known to be a CO-induced ferroelectric with switchable polarization [5,6,37,38]. Below the Verwey temperature $T_V = 125$ K, Fe_3O_4 adopts a monoclinic Cc structure [49]. Previous first-principles calculations have located the Fe^{2+} and Fe^{3+} at the 16 inequivalent six-fold sites of this structure and shown that they are noncentrosymmetrically arranged [6], leading to a nonzero polarization (see SM Sec. VII for the structure). In Fig. 4(c), we plot the Q_{PB} and Q_{OD} of these 16 Fe ions, in descending order of their Q_{PB} . We note that the eight Fe^{2+} ions have positive Q_{PB} and eight Fe^{3+} ions have negative Q_{PB} [6], which indicates that the PB modes for these polyhedra are strongly coupled to the CO state. We now focus on the pair of ions in the middle of the range in Fig. 4(c), one Fe^{2+} and one Fe^{3+} , which we note are neighboring in the crystal structure (see SM Sec. VII). The change of polarization due to the valence switching of this pair of Fe ions is $3 \mu\text{C}/\text{m}^2$, the same order of magnitude as the experimental result ($5 \mu\text{C}/\text{m}^2$ in Ref. [50]). They have quite similar Q_{PB} and noticeably different Q_{OD} with opposite signs, analogous to the constrained $(\text{SrVO}_3)_1(\text{LaVO}_3)_1$ superlattice with $R = 1$. In this case, the PB mode appears to be suppressed, so that according to our analysis above, ΔE is expected to be small, opening the possibility of nonadiabatic switching. To confirm our hypothesis, we carry out first-principles calculations and find that ΔE is approximately zero (4 meV/cell), indicating that the structure has two stable/metastable electronic states with quite similar energies. Even though the observed polarization switching in Fe_3O_4 could be a complex process which might involve both the effects of lattice relaxation and electron hopping, our structural analysis and first-principles calculations indicate that nonadiabatic switching is a possible switching mechanism in Fe_3O_4 .

In this work, we focus on the nonadiabatic switching in CO-induced ferroelectrics because we are interested in polarization switching on electronic time scales, which are much faster than the lattice-relaxation time scales. At longer time scales, an electric field and thermal vibrations can lead

to atomic displacements, which could lower ΔE and assist switching. The PB mode does not couple linearly to an applied electric field and thus changes little under an electric field (see SM Sec. VIII for more discussion). The OD mode is infrared active and responds more strongly to an electric field. However, the reductions of ΔE and threshold electric field due to the change of the OD mode are found to be small (see SM Sec. IX for more discussion).

IV. CONCLUSION

In summary, we investigate the coupling between electronic state and lattice mode in charge-order-induced ferroelectrics and propose a theoretical model predicting the possibility of nonadiabatic polarization switching from structural analysis. Specifically, we demonstrate that the nonadiabatic polarization switchability depends on the type of lattice distortion, polyhedral breathing or off-centering displacement mode, which primarily couples to the CO state. Nonadiabatic switching is possible only in a system that has at least a subset of sites for which the strongest coupling is

to the off-centering displacements rather than to the polyhedral breathing. This work presents an understanding of the polarization switching mechanism in charge-order-induced ferroelectrics by emphasizing the critical role of the coupling between the charge-ordering state and the lattice modes. It offers an explanation for why the polarization in some proposed charge-order-induced “electronic ferroelectrics” cannot in fact be switched by an electric field, and provides valuable insights and strategies for the design and discovery of electronic ferroelectrics with polarization switching on electronic time scales.

ACKNOWLEDGMENTS

We thank Cyrus Dreyer for valuable discussions. This work was supported by Office of Naval Research N00014-21-1-2107. First-principles calculations were performed using the computational resources provided by the Rutgers University Parallel Computing (RUPC) clusters and the High-Performance Computing Modernization Office of the Department of Defense.

-
- [1] M. Imada, A. Fujimori, and Y. Tokura, *Rev. Mod. Phys.* **70**, 1039 (1998).
 - [2] D. V. Efremov, J. van den Brink, and D. I. Khomskii, *Nat. Mater.* **3**, 853 (2004).
 - [3] J. van den Brink and D. I. Khomskii, *J. Phys.: Condens. Matter* **20**, 434217 (2008).
 - [4] K. Kobayashi, S. Horiuchi, R. Kumai, F. Kagawa, Y. Murakami, and Y. Tokura, *Phys. Rev. Lett.* **108**, 237601 (2012).
 - [5] M. Alexe, M. Ziese, D. Hesse, P. Esquinazi, K. Yamauchi, T. Fukushima, S. Picozzi, and U. Gösele, *Adv. Mater.* **21**, 4452 (2009).
 - [6] K. Yamauchi, T. Fukushima, and S. Picozzi, *Phys. Rev. B* **79**, 212404 (2009).
 - [7] J. B. Goodenough, *Phys. Rev.* **100**, 564 (1955).
 - [8] A. Daoud-Aladine, J. Rodriguez-Carvajal, L. Pinsard-Gaudart, M. T. Fernandez-Diaz, and A. Revcolevschi, *Phys. Rev. Lett.* **89**, 097205 (2002).
 - [9] D. V. Efremov, J. van den Brink, and D. I. Khomskii, *Phys. B: Condens. Matter* **359-361**, 1433 (2005).
 - [10] S. Mercone, A. Wahl, A. Pautrat, M. Pollet, and C. Simon, *Phys. Rev. B* **69**, 174433 (2004).
 - [11] C. Jardón, F. Rivadulla, L. Hueso, A. Fondado, M. A. Lopez-Quintela, J. Rivas, R. Zysler, M. T. Causa, and R. D. Sanchez, *J. Magn. Magn. Mater.* **196-197**, 475 (1999).
 - [12] E. O. Wollan and W. C. Koehler, *Phys. Rev.* **100**, 545 (1955).
 - [13] S. Grenier, J. P. Hill, D. Gibbs, K. J. Thomas, M. v. Zimmermann, C. S. Nelson, V. Kiryukhin, Y. Tokura, Y. Tomioka, D. Casa, T. Gog, and C. Venkataraman, *Phys. Rev. B* **69**, 134419 (2004).
 - [14] L. Wu, R. F. Klie, Y. Zhu, and C. Jooss, *Phys. Rev. B* **76**, 174210 (2007).
 - [15] J. A. Alonso, J. L. García-Muñoz, M. T. Fernández-Díaz, M. A. G. Aranda, M. J. Martínez-Lope, and M. T. Casais, *Phys. Rev. Lett.* **82**, 3871 (1999).
 - [16] T. Mizokawa, D. I. Khomskii, and G. A. Sawatzky, *Phys. Rev. B* **61**, 11263 (2000).
 - [17] A. B. Harris, *Phys. Rev. B* **76**, 054447 (2007).
 - [18] I. Kagomiya, S. Matsumoto, K. Kohn, Y. Fukuda, T. Shoubu, H. Kimura, Y. Noda, and N. Ikeda, *Ferroelectrics* **286**, 167 (2003).
 - [19] N. Hur, S. Park, P. Sharma, J. Ahn, S. Guha, and S.-W. Cheong, *Nature (London)* **429**, 392 (2004).
 - [20] J. J. Betouras, G. Giovannetti, and J. van den Brink, *Phys. Rev. Lett.* **98**, 257602 (2007).
 - [21] L. C. Chapon, G. R. Blake, M. J. Gutmann, S. Park, N. Hur, P. G. Radaelli, and S.-W. Cheong, *Phys. Rev. Lett.* **93**, 177402 (2004).
 - [22] G. R. Blake, L. C. Chapon, P. G. Radaelli, S. Park, N. Hur, S.-W. Cheong, and J. Rodriguez-Carvajal, *Phys. Rev. B* **71**, 214402 (2005).
 - [23] C. Wang, G.-C. Guo, and L. He, *Phys. Rev. Lett.* **99**, 177202 (2007).
 - [24] J. S. Lim, D. Saldana-Greco, and A. M. Rappe, *Phys. Rev. B* **97**, 045115 (2018).
 - [25] S. Y. Park, A. Kumar, and K. M. Rabe, *Phys. Rev. Lett.* **118**, 087602 (2017).
 - [26] S. Y. Park, K. M. Rabe, and J. B. Neaton, *Proc. Natl. Acad. Sci. USA* **116**, 23972 (2019).
 - [27] A. L. Krick, C.-W. Lee, R. J. Sichel-Tissot, A. M. Rappe, and S. J. May, *Adv. Electron. Mater.* **2**, 1500372 (2016).
 - [28] S. Ishihara, *J. Phys. Soc. Jpn.* **79**, 011010 (2010).
 - [29] K. Yamauchi and P. Barone, *J. Phys.: Condens. Matter* **26**, 103201 (2014).
 - [30] N. Ikeda, H. Ohsumi, K. Ohwada, K. Ishii, T. Inami, K. Kakurai, Y. Murakami, K. Yoshii, S. Mori, Y. Horibe *et al.*, *Nature (London)* **436**, 1136 (2005).
 - [31] N. Ikeda, *J. Phys.: Condens. Matter* **20**, 434218 (2008).
 - [32] H. J. Xiang and M.-H. Whangbo, *Phys. Rev. Lett.* **98**, 246403 (2007).

- [33] H. J. Xiang, E. J. Kan, S.-H. Wei, M.-H. Whangbo, and J. Yang, *Phys. Rev. B* **80**, 132408 (2009).
- [34] J. de Groot, T. Mueller, R. A. Rosenberg, D. J. Keavney, Z. Islam, J.-W. Kim, and M. Angst, *Phys. Rev. Lett.* **108**, 187601 (2012).
- [35] S. Lafuerza, J. García, G. Subías, J. Blasco, K. Conder, and E. Pomjakushina, *Phys. Rev. B* **88**, 085130 (2013).
- [36] A. Ruff, S. Krohns, F. Schrettle, V. Tsurkan, P. Lunkenheimer, and A. Loidl, *Eur. Phys. J. B* **85**, 290 (2012).
- [37] K. Yamauchi and S. Picozzi, *J. Phys. Soc. Jpn.* **82**, 113703 (2013).
- [38] M. S. Senn, J. P. Wright, and J. P. Attfield, *Nature (London)* **481**, 173 (2012).
- [39] P. V. Balachandran and J. M. Rondinelli, *Phys. Rev. B* **88**, 054101 (2013).
- [40] N. C. Bristowe, J. Varignon, D. Fontaine, E. Bousquet, and P. Ghosez, *Nat. Commun.* **6**, 6677 (2015).
- [41] J. Matsuno, T. Mizokawa, A. Fujimori, Y. Takeda, S. Kawasaki, and M. Takano, *Phys. Rev. B* **66**, 193103 (2002).
- [42] See Supplemental Material at <http://link.aps.org/supplemental/10.1103/PhysRevB.106.125131> for information regarding the computational method, structures, stabilities of difference co-patterns, occupation matrices, and responses of lattice modes with electric fields. See also Refs. [25,33,43,44,49,51–62].
- [43] Q. Han and A. Millis, *Phys. Rev. Lett.* **121**, 067601 (2018).
- [44] A. B. Georgescu, O. E. Peil, A. S. Disa, A. Georges, and A. J. Millis, *Proc. Natl. Acad. Sci. USA* **116**, 14434 (2019).
- [45] A. B. Georgescu and A. J. Millis, [arXiv:2105.02271](https://arxiv.org/abs/2105.02271) (2021).
- [46] R. V. Shende, D. S. Krueger, G. A. Rossetti, and S. J. Lombardo, *J. Am. Ceram. Soc.* **84**, 1648 (2001).
- [47] I. Ueda, M. Takiuchi, S. Ikegami, and H. Sato, *J. Phys. Soc. Jpn.* **19**, 1267 (1964).
- [48] M. Isobe, N. Kimizuka, J. Iida, and S. Takekawa, *Acta Crystallogr. Sect. C* **46**, 1917 (1990).
- [49] E. J. W. Verwey, *Nature (London)* **144**, 327 (1939).
- [50] M. Ziese, P. D. Esquinazi, D. Pantel, M. Alexe, N. M. Nemes, and M. Garcia-Hernández, *J. Phys.: Condens. Matter* **24**, 086007 (2012).
- [51] P. Giannozzi, S. Baroni, N. Bonini, M. Calandra, R. Car, C. Cavazzoni, D. Ceresoli, G. L. Chiarotti, M. Cococcioni, I. Dabo, A. D. Corso, S. de Gironcoli, S. Fabris, G. Fratesi, R. Gebauer, U. Gerstmann, C. Gougoussis, A. Kokalj, M. Lazzeri, L. Martin-Samos *et al.*, *J. Phys.: Condens. Matter* **21**, 395502 (2009).
- [52] A. I. Liechtenstein, V. I. Anisimov, and J. Zaanen, *Phys. Rev. B* **52**, R5467 (1995).
- [53] H. Sawada, N. Hamada, K. Terakura, and T. Asada, *Phys. Rev. B* **53**, 12742 (1996).
- [54] Z. Fang, N. Nagaosa, and K. Terakura, *Phys. Rev. B* **67**, 035101 (2003).
- [55] S. Biermann, A. Poteryaev, A. I. Lichtenstein, and A. Georges, *Phys. Rev. Lett.* **94**, 026404 (2005).
- [56] M. T. Czyżyk and G. A. Sawatzky, *Phys. Rev. B* **49**, 14211 (1994).
- [57] H. J. Monkhorst and J. D. Pack, *Phys. Rev. B* **13**, 5188 (1976).
- [58] R. D. King-Smith and D. Vanderbilt, *Phys. Rev. B* **47**, 1651 (1993).
- [59] I. Souza, J. Íñiguez, and D. Vanderbilt, *Phys. Rev. Lett.* **89**, 117602 (2002).
- [60] X. Wang and D. Vanderbilt, *Phys. Rev. B* **75**, 115116 (2007).
- [61] X. Wang and D. Vanderbilt, *Phys. Rev. B* **74**, 054304 (2006).
- [62] L. Bellaïche, A. García, and D. Vanderbilt, *Phys. Rev. B* **64**, 060103(R) (2001).